Detection of Broadband Terahertz Waves with a Laser-Induced Plasma in Gases

Jianming Dai, Xu Xie, and X.-C. Zhang*

Center for Terahertz Research, Rensselaer Polytechnic Institute, Troy, New York 12180, USA
(Received 25 April 2006; published 8 September 2006)

We report the experimental results and theoretical analysis of broadband detection of terahertz (THz) waves via electric-field-induced second-harmonic generation in laser-induced air plasma with ultrashort laser pulses. By introducing the second-harmonic component of the white light in the laser-induced plasma as a local oscillator, coherent detection of broadband THz waves with ambient air is demonstrated for the first time. Our results show that, depending on the probe intensity, detection of THz waves in air can be categorized as incoherent, hybrid, and coherent detection. Coherent detection is achieved only when the tunnel ionization process dominates in gases.

Coherent detection with a simultaneous measurement of the amplitude and phase of a pulsed terahertz (THz) wave is the basis of time-domain spectroscopy (TDS), which has become one of the most active spectroscopic methods in the physics and material science communities [1]. It provides dynamic properties of various dielectric materials over the frequency range from 0.1 to 10 THz, which was previously considered to be a difficult-to-access range. For example, the unique features of this coherent and time-resolved method provided direct measurement of dynamic formation of Drude model in photoexcited Coulomb dressed free carriers [2]. Commonly used coherent detectors for detecting THz waves in the THz TDS are photoconductive dipole antennas and electro-optic crystals [3,4]. However, their bandwidth is limited by the carrier lifetime in semiconducting photoconductors and phonon absorption in electro-optic crystals.

In this Letter, we present theoretical analysis and experimental demonstration of both incoherent and coherent detection of broadband THz waves using gases as the sensor medium through a third-order nonlinear optical process with femtosecond (fs) laser pulses. We demonstrate that the field-induced second harmonic from the nonlinear optical interaction in the air offers time-resolved measurement of pulsed THz waves. By using the white light from the laser-induced plasma as the local oscillator (LO), the detection could be coherent. Furthermore, by increasing the probe beam intensity, the detection changes from incoherent detection at lower intensities to coherent detection at higher intensities. Correspondingly, the laser-induced ionization of the gas changes from multiphoton ionization (MI) to tunnel ionization (TI), which is indicated by the Keldysh parameter γ [5,6].

Gases, especially ionized gases, have been demonstrated to generate intense THz waves through laser-induced ponderomotive forces [7], Lorentz forces [8], and third-order nonlinear optical processes [9–12]. Similar to the electro-optic detection of THz waves in nonlinear crystals by second-order optical nonlinearity, THz waves can be detected by third-order optical nonlinearity. Ambient air,

with a composition of about 78% nitrogen, exhibits remarkable performance for the generation and detection of THz waves with fs laser pulses.

Experimentally, a Ti:sapphire amplifier, generating 800 nm, 120 fs, 800 μJ pulses at a repetition rate of 1 kHz, is used. The laser beam is split into two beams. One beam is used to generate THz waves, and the other is used to detect the THz waves. Figure 1 schematically illustrates this all-optical process for the generation and detection of THz waves using air as the emitter and sensor. First, the fundamental (ω) beam and its SH (2ω), after passing through a 100 μm thick type-I beta barium borate (BBO) crystal, are focused in air to produce plasma [9]. An
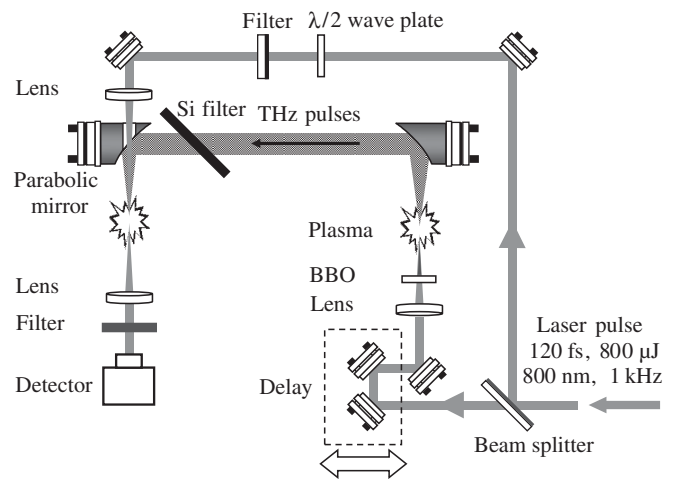

FIG. 1. Schematic diagram of the experimental setup. The THz wave is generated by mixing the ω pump beam and its SH (from a type-I BBO crystal) at the first air plasma point. The first parabolic mirror collimates the THz beam. A high-resistivity silicon wafer blocks the residual 800 and 400 nm beams. The second parabolic mirror focuses the collimated THz beam. A $\lambda/2$ wave plate controls the polarization of the probe beam. The THz wave is detected by measuring the time-resolved SH signal produced by mixing the ω beam and the THz field at the second plasma point.

intense, highly directional, broadband THz wave is generated through four-wave mixing [11,12]. Detailed experimental results regarding the nonlinear process for the THz wave generation in air plasma are demonstrated in our previous publication [13], and references therein. To detect the THz waves in air, the THz wave and the probe beam are focused at the same point, with estimated focal spots of about 0.8 mm and 24 μm in diameter, respectively. The THz-field-induced second harmonic (TFISH) is detected by a photomultiplier tube.

We measured time-resolved TFISH signals at different probe intensities. To eliminate the water vapor absorption, the entire THz system is purged with nitrogen gas. As the probe intensity increases from 9.2×10^{12} to 1.0×10^{15} W/cm^2 while the THz field is kept the same, the detected SH signal increases accordingly while the waveform is kept the same with a unipolar feature until the probe intensity reaches $\sim 1.8 \times 10^{14}$ W/cm^2. Above this intensity level, the waveform begins to change, and especially above 3.3×10^{14} W/cm^2, the measured SH waveform starts to change from the unipolar shape to bipolar. Figure 2 shows a typical unipolar waveform of incoherent measurement (upper), a bipolar waveform of coherent measurement (lower), and a waveform between them (middle), with their offsets shifted for clarity. When the probe intensity is over $\sim 5.5 \times 10^{14}$ W/cm^2, the SH waveforms are nearly identical to those detected by the ZnTe crystal, indicating the coherent detection of the THz waves.

In the reciprocal process of four-wave rectification, the general physical concept of TFISH in third-order nonlinearity [14,15] can be understood as:

$$E_{2\omega}^{signal} \propto \chi^{(3)} E_\omega E_\omega E_{THz}, \qquad (1)$$

where $\chi^{(3)}$ is the third-order susceptibility of air, and E is

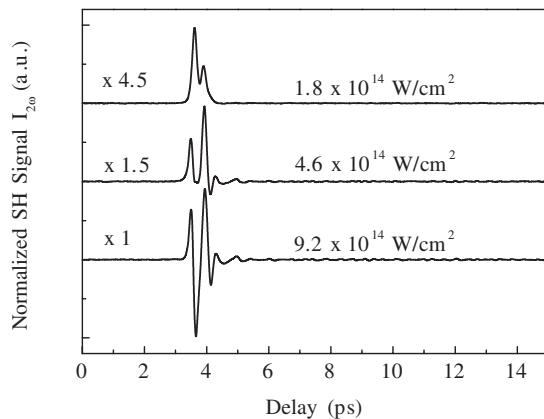

FIG. 2. Typical time-resolved SH waveforms (solid lines) measured with a gas sensor at three different estimated probe intensities: 1.8×10^{14} W/cm^2 (upper), 4.6×10^{14} W/cm^2 (middle), and 9.2×10^{14} W/cm^2 (lower), respectively. The waveform offsets are shifted for clarity.

the electric field component associated with the optical field or THz field. Since $E_{2\omega}^{signal} \propto E_{THz}$, the intensity of the measured SH is proportional to the intensity of the THz wave: $I_{2\omega} \propto I_{THz}$. The phase information is lost; therefore, the measurement is incoherent.

When the SH LO contribution $E_{2\omega}^{LO}$ is included into the analysis, the total SH intensity in the time average values over one period of E-field oscillation has the form:

$$I_{2\omega} \propto (E_{2\omega})^2 = (E_{2\omega}^{signal} + E_{2\omega}^{LO})^2$$
$$= (E_{2\omega}^{signal})^2 + (E_{2\omega}^{LO})^2 + 2E_{2\omega}^{signal} E_{2\omega}^{LO} \cos(\varphi), \qquad (2)$$

where φ is the phase difference between the $E_{2\omega}^{signal}$ and $E_{2\omega}^{LO}$. The LO $E_{2\omega}^{LO}$ is contributed from the white light generated from the laser-induced air plasma through self-phase modulation and self-steepening, and it depends on plasma density, especially in the transition from ambient air to ionized air, and, accordingly, the LO should have a well-defined threshold. Equation (2) can be written as:

$$I_{2\omega} \propto (\chi^{(3)} I_\omega)^2 I_{THz} + (E_{2\omega}^{LO})^2 + 2\chi^{(3)} I_\omega E_{2\omega}^{LO} E_{THz} \cos(\varphi). \qquad (3)$$

The first term is proportional to the intensity of the THz wave. With a zero or a weak LO (small $E_{2\omega}^{LO}$), the first term is dominant, leading to $I_{2\omega} \propto I_{THz}$. The second term is the dc contribution from the LO and can be filtered out through the use of a lock-in amplifier by modulating the THz beam. The third term is the interference term, which is proportional to E_{THz}. This term provides the basis of coherent detection. With the above approximations, Eq. (3) can be simplified to the form:

$$I_{2\omega} \propto (\chi^{(3)} I_\omega)^2 I_{THz} + 2\chi^{(3)} I_\omega E_{2\omega}^{LO} E_{THz} \cos(\varphi). \qquad (4)$$

Equation (4) is obtained from the plane-wave approximation. It should be pointed out that $\chi^{(3)}$ could be probe intensity dependent, especially when the probe intensity approaches the plasma threshold. A constant φ is a good approximation because we experimentally proved that, in our setup, the only source for the SH LO is the 2ω component of the white light, which has a fixed phase relationship with the ω beam when the probe energy is fixed.

Equation (4) predicts that $I_{2\omega} \propto I_{THz}$ without a LO or $I_{2\omega} \propto E_{THz}$ with a strong LO. With probe intensity less than the air ionization threshold, the LO $E_{2\omega}^{LO}$ is negligible, and the total SH is dominated by the first term in Eq. (4); therefore, the measured $I_{2\omega}$ is unipolar, and the detection is incoherent. With the probe intensity much higher than the plasma threshold, the second term dominates. $I_{2\omega}$ is proportional to the THz electric field with a bipolar waveform, and the detection is coherent. The measured $I_{2\omega}$ waveforms at three different probe intensities indicated in Fig. 2 qualitatively agree well with the predication in Eq. (4).
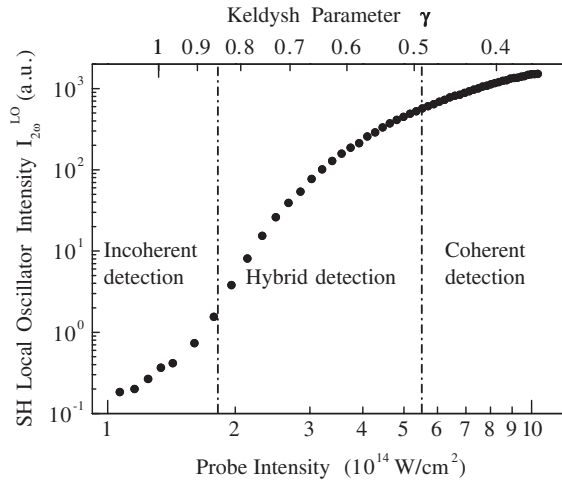
FIG. 3.   Local oscillator intensity $I_{2\omega}^{LO}$ vs probe intensity in log-log scale (solid dots). The local oscillator intensity becomes significant after the probe intensity is greater than 1.8×10^{14} W/cm^2. The corresponding Keldysh parameters γ are indicated on the upper axis. The entire probe intensity range is divided into three subranges, which are experimentally defined as incoherent, hybrid, and coherent detection, respectively, with two vertical dashed-dotted lines.

To verify the LO $E_{2\omega}^{LO}$ and its contribution following different probe intensities, we measured the dc term $(E_{2\omega}^{LO})^2$ in Eq. (3) by modulating the probe beam while blocking the THz beam. Figure 3 plots the intensity of total SH LO $(I_{2\omega}^{LO})$ versus the estimated probe intensity on a log-log scale. The SH LO does not become significant until the probe intensity reaches $\sim 1.8 \times 10^{14}$ W/cm^2. After that, the intensity of SH LO increases dramatically with the probe intensity. When the probe intensity reaches over $\sim 5.5 \times 10^{14}$ W/cm^2, the increase of the LO intensity slows down with an average slope of ~ 1.5.
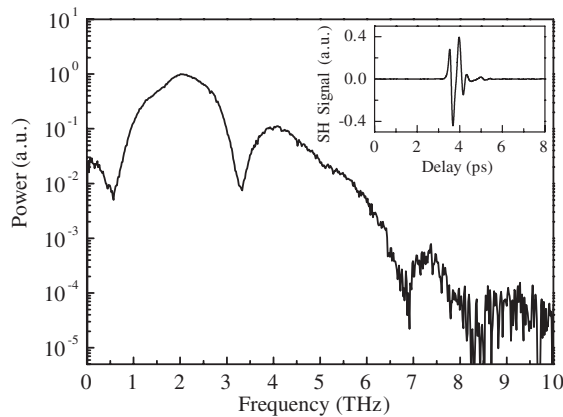

FIG. 4.   Detected THz waveform in the time domain (inset) using nitrogen gas as the sensor and the corresponding THz spectrum obtained from the discrete Fourier transform of the THz waveform. The waveform, measured by a field-induced-second-harmonic signal $I_{2\omega}$ in air, shows the coherent nature which measures both the amplitude and phase of THz pulses.

To identify these different processes, we indicate the Keldysh parameter γ at different probe intensities in Fig. 3. Meanwhile, we define three different detection regimes, i.e., incoherent, hybrid, and coherent detection,
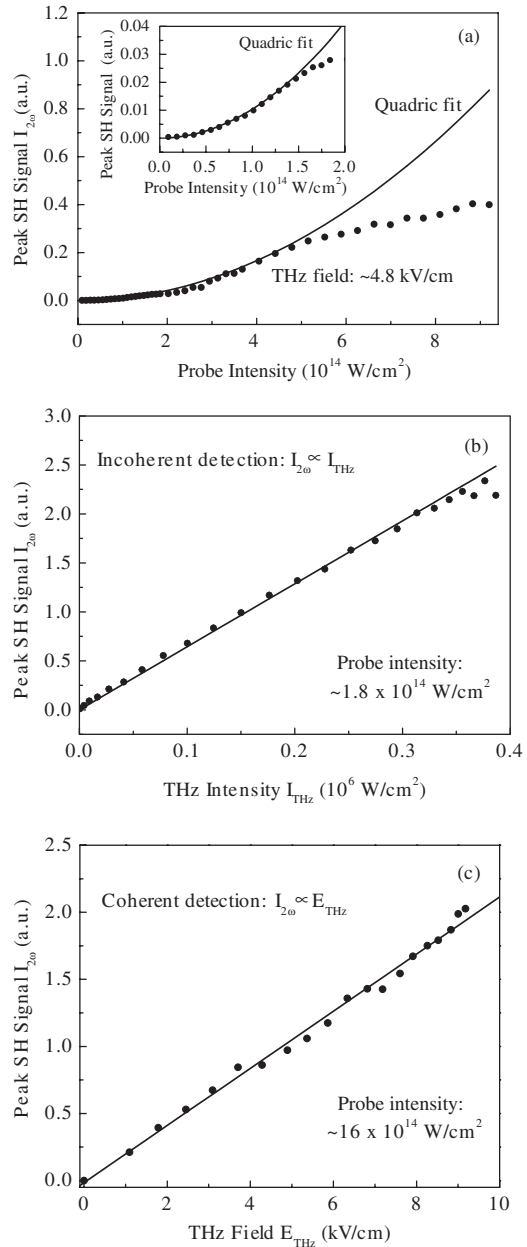

FIG. 5.   (a) Measured SH intensity $I_{2\omega}$ versus the probe beam intensity I_ω (solid dots). When the probe intensity is below the plasma threshold ($\sim 1.8 \times 10^{14}$ W/cm^2), the data fit well to a quadratic function (solid line). (b) Measured $I_{2\omega}$ versus the THz intensity I_{THz} when the probe intensity is fixed at 1.8×10^{14} W/cm^2 (solid dots). The solid line is a linear fit. (c) Measured $I_{2\omega}$ versus THz electric field strength E_{THz} when the probe intensity is fixed at $\sim 16 \times 10^{14}$ W/cm^2 (solid dots). The solid line is a linear fit. Note that shorter focal lengths of the parabolic mirror and probe focal lens are used to increase the dynamic range of the measurement.

according to the waveforms obtained at different probe intensities. The boundary between incoherent and hybrid detection is reasonably located around the white light plasma threshold. The defined boundary between hybrid and coherent detection is close to the transition condition between MI and TI, i.e., $\gamma = 1/2$, which was previously required to be $\gamma \ll 1$ by Keldysh theory and modified to $\gamma < 1/2$ for the TI in the fs region [6]. The plasma formation directly gives rise to a change of the refractive index and causes a spectral broadening towards the blue side of the pump frequency [16]. The intensity of the 400 nm component of white light increases due to the further spectral broadening towards the blue as the plasma density increases. Apparently, the fast increase of SH LO in the hybrid detection region is due to MI, which cannot yield very strong plasma because of the fs pulse duration. In MI, the SH component (LO) of the white light increases very fast so that the second term in Eq. (4) increases much faster than the first term until TI dominates, at which point the LO becomes very strong and the second term in Eq. (4) dominates. In other words, only when TI dominates the process can the total LO be strong enough to lead to coherent detection.

The highest dynamic range of the coherent detection demonstrated is over 10^3, with a lock-in time constant of 0.3 s. Figure 4 plots a typical spectrum and its waveform (inset) with the air-breakdown-coherent detection when the THz wave is generated and detected in nitrogen gas. In Fig. 4, we observed dips at 0.5 and 3.25 THz. At this moment, we cannot identify the origin of dips. However, the dips shift slightly and even disappear with different probe intensities.

Figure 5(a) shows a quadric dependence of the peak SH signal on probe intensity when it is below $\sim 1.8 \times 10^{14}$ W/cm^2 while the THz field is kept at ~ 4.8 kV/cm; when the probe intensity is over 1.8×10^{14} W/cm^2, the variation of the peak SH signal with probe intensity becomes complicated due to the simultaneous existence of incoherent and coherent detection. Figure 5(b) shows a linear dependence of peak SH signals on the THz intensity when the probe intensity is fixed at $\sim 1.8 \times 10^{14}$ W/cm^2. Figures 5(a) and 5(b) verified the validity of the first term in Eq. (4) for incoherent detection. In the case of coherent detection, we need to verify $I_{2\omega} \propto E_{THz}$, i.e., the second term in Eq. (4). To ensure that the probe beam has enough intensity at the focal spot while maintaining adequate dynamic range in the pump beam, we reduced the focal lengths of the probe lens and the parabolic mirror near the probe and fixed the probe intensity at $\sim 16 \times 10^{14}$ W/cm^2.

Figure 5(c) plots $I_{2\omega}$ versus E_{THz}, with a linear relationship between $I_{2\omega}$ and E_{THz}. The results agree well with Eq. (4).

In conclusion, we report the first demonstration of broadband THz wave detection through third-order nonlinear optical processes using gases as the sensor. Our results show that, when the probe intensity is below the white light plasma threshold, the detection is completely incoherent; above the threshold, but when the ionization is dominated by multiphoton processes, both incoherent and coherent detection exist simultaneously; we defined this case as hybrid detection; when the probe intensity is well above the threshold, TI dominates the process, and the detection is coherent. We proposed that coherent detection using gases as the sensor medium is achieved only when the TI process dominates. The demonstration offers great flexibility in the choice of sensing location, since air is one of the most readily available resources in free space. This all-air, all-optical approach could send optical beams to generate and detect THz waves locally, utilizing a lower attenuation at the visible range (< 0.01 dB/km) in ambient air. Air-breakdown-coherent detection will enable THz wave remote sensing and spectroscopy, which was previously considered impossible.

*Electronic address: zhangxc@rpi.edu
[1] B. Ferguson and X.-C. Zhang, Nat. Mater. **1**, 26 (2002).
[2] R. Huber *et al.*, Nature (London) **414**, 286 (2001).
[3] D. Grischkowsky *et al.*, J. Opt. Soc. Am. B **7**, 2006 (1990).
[4] Q. Wu and X.-C. Zhang, Appl. Phys. Lett. **67**, 3523 (1995).
[5] L. V. Keldysh, Sov. Phys. JETP **20**, 1307 (1965).
[6] T. D. G. Walsh *et al.*, J. Phys. B **27**, 3767 (1994).
[7] H. Hamster *et al.*, Phys. Rev. Lett. **71**, 2725 (1993).
[8] S. Tzortzakis *et al.*, Opt. Lett. **27**, 1944 (2002).
[9] D. J. Cook and R. M. Hochstrasser, Opt. Lett. **25**, 1210 (2000).
[10] M. Kress *et al.*, Opt. Lett. **29**, 1120 (2004).
[11] T. Löffler *et al.*, Acta Phys. Pol. A **107**, 99 (2005).
[12] T. Bartel *et al.*, Opt. Lett. **30**, 2805 (2005).
[13] X. Xie, J. Dai, and X.-C. Zhang, Phys. Rev. Lett. **96**, 075005 (2006).
[14] A. Nahata and T. F. Heinz, Opt. Lett. **23**, 67 (1998).
[15] D. J. Cook *et al.*, Chem. Phys. Lett. **309**, 221 (1999).
[16] S. L. Chin *et al.*, Can. J. Phys. **83**, 863 (2005).